

## Article

# Design of an Adaptive Distributed Drive Control Strategy for a Wheel-Side Rear-Drive Electric Bus

Huipeng Chen <sup>1</sup>, Weiyang Wang <sup>1</sup>, Shaopeng Zhu <sup>2</sup>, Sen Chen <sup>1</sup>, Jian Gao <sup>3</sup>, Rougang Zhou <sup>1,4,5</sup> and Wei Wei <sup>6,\*</sup><sup>1</sup> School of Mechanical Engineering, Hangzhou Dianzi University, Hangzhou 310005, China<sup>2</sup> Power Machinery & Vehicular Engineering Institute, College of Energy Engineering, Zhejiang University, Hangzhou 310058, China<sup>3</sup> Polytechnic Institute, Zhejiang University, 866 Yuhangtang Rd, Hangzhou 310058, China<sup>4</sup> Wenzhou Institute of Hangzhou Dianzi University, Wenzhou 325013, China<sup>5</sup> Mstar Technologies, Inc., Hangzhou 310012, China<sup>6</sup> College of Information Engineering, Zhejiang University of Water Resources and Electric Power, Hangzhou 310018, China

\* Correspondence: weiw@zjweu.edu.cn; Tel.: +86-13819173537

**Abstract:** A wheel motor simplifies the chassis structure of an electric bus, greatly improving its response speed and controllability. How to improve the lateral stability of the vehicle under complex and changeable driving conditions is a major problem in the motion control of electric buses. This study proposed an adaptive distributed drive control strategy for a rear-wheel drive electric bus. An adaptive fuzzy controller was designed to obtain the additional yaw moment of the vehicle and then combined with a rule distribution method to modify the steering characteristics of the vehicle to obtain the optimal driving torque distribution. Hardware-in-the-loop test results showed that under adaptive fuzzy control, the yaw rate deviations under low- and high-speed conditions were reduced from 18% and 42% without control to 10% and 23% with control, respectively. Under sine wave conditions, the deviation of the yaw rate and the vehicle's sideslip angle were reduced from 83% and 852% without control to 12% and 15% with control, respectively. It was verified that the electric bus with adaptive fuzzy control could maintain good vehicle stability at full speed.

**Keywords:** electric bus; yaw moment control; adaptive fuzzy control; distributed drive; lateral stability



**Citation:** Chen, H.; Wang, W.; Zhu, S.; Chen, S.; Gao, J.; Zhou, R.; Wei, W. Design of an Adaptive Distributed Drive Control Strategy for a Wheel-Side Rear-Drive Electric Bus. *Electronics* **2022**, *11*, 4223. <https://doi.org/10.3390/electronics11244223>

Academic Editor: Boris Andrievsky

Received: 21 October 2022

Accepted: 13 December 2022

Published: 18 December 2022

**Publisher's Note:** MDPI stays neutral with regard to jurisdictional claims in published maps and institutional affiliations.



**Copyright:** © 2022 by the authors. Licensee MDPI, Basel, Switzerland. This article is an open access article distributed under the terms and conditions of the Creative Commons Attribution (CC BY) license (<https://creativecommons.org/licenses/by/4.0/>).

## 1. Introduction

In recent years, with the gradual improvement in automobile technology and power performance, more and more automobile users' concerns have shifted from vehicle performance to vehicle driving safety. Therefore, the major commercial vehicle manufacturers have gradually focused more of their attention on how to improve the safety of city buses. The automotive electronic stability program (ESP) [1] is a multifunctional active safety device that can greatly improve a vehicle's steering safety through direct yaw moment control (DYC) and is also an important part of the active safety control system [2,3]. To directly realize the yawing moment and control, the distributed drive control of electric vehicles uses independent control of the torque of each wheel, uses the car driving force theory to reasonably allocate direct yawing moment control, and does not involve the use of the vehicle's braking; this is in contrast to traditional centralized fuel vehicles, which directly use differential braking to provide yawing moment control. From the perspective of vehicle stability, response speed, and control accuracy, the method of adjusting the driving force of each wheel of a distributed drive vehicle is better than the method of centralized control of a centralized drive vehicle. At present, the methods of direct yaw moment control in automobiles are sliding mode control [4], PID control [5], fuzzy control [6], and model predictive control [7]. Among them, fuzzy control has the advantages of not relying

on specific control objects and good robustness, and thus, it is the most widely used in automobile control.

Many scholars studied the motion tracking control algorithm in the distributed drive control strategy [8], which primarily includes feedback linearization control, PI control, and feedforward plus dynamic sliding mode feedback control. The feedback linearization control algorithm is used in the design of the yaw rate tracking controller by eliminating the nonlinear parts of the nonlinear system and linearizing the rest of the system. The algorithm can avoid the influence of nonlinear parts of the vehicle system on the control effect, but for some control objects with unclear vehicle parameters, the control effect is poor and the applicability is narrow [6]. In the PI control algorithm, the deviation between the actual yaw velocity and the ideal yaw velocity obtained from the vehicle's two-degrees-of-freedom model is taken as the input, and the yaw moment corrected by the deviation is obtained through the PI controller. The control algorithm is simple and reliable and is suitable for the linear constant system of the accurate mathematical model. However, there is evident nonlinearity and complexity in the vehicle system. Therefore, the PI controller will have significant differences in the control effects in different working conditions [9–11]. The feedforward plus optimal dynamic sliding mode feedback control was proposed in reference [12]. The vehicle's actual yaw rate  $\omega$  and ideal yaw rate  $\omega_d$  derived from the improved two-degrees-of-freedom reference model was used as the dynamic sliding mode feedback control input, and at the same time, the front wheel angle and vehicle speed were used as the feedforward control inputs and outputs of the yaw moments. The control algorithm has low requirements regarding the vehicle model precision and wide adaptation, but due to the limitations of the sliding mode control itself, if the switching function is not properly designed, high-frequency jitter will inevitably appear on the switching surface [13].

In this study, taking a distributed rear-drive electric bus as the research object, based on the characteristics that the driving torque of each driving wheel can be controlled independently, an adaptive fuzzy control algorithm based on the direct yaw moment control principle was proposed to improve the vehicle's lateral stability. The main work had the following three aspects: (1) An adaptive distributed drive control system with a hierarchical control structure was proposed for a rear-drive electric bus, including an additional yaw moment setting layer and a driving torque distribution layer. (2) In the additional yaw moment setting layer, an adaptive fuzzy controller was designed based on the principle of direct yaw moment control. The yaw rate deviation and the vehicle's sideslip angle deviation between the actual value and the expected value were calculated as the inputs of the controller. By dynamically adjusting the quantization factor and scale factor of the fuzzy control, the adaptive fuzzy controller can set the optimal additional yaw moment to improve vehicle stability. (3) Using an NI PXIE-880 real-time processor and a DSP28335 controller, a hardware-in-the-loop test platform was built. The hardware-in-the-loop test of the proposed adaptive drive control strategy was carried out under different working conditions.

## 2. Build Dynamics Models

To design the adaptive distributed drive control strategy and verify it, it was necessary to establish a two-degrees-of-freedom vehicle reference model and a five-degrees-of-freedom vehicle dynamics model using TruckSim software (TruckSim 2020).

### 2.1. Reference Model

A vehicle's attitude and running trajectory are important factors to consider in vehicle lateral stability. A vehicle's yaw angle and yaw velocity are the two main parameters that represent the vehicle's stability and running trajectory. Therefore, a linear two-degrees-of-freedom vehicle reference model was established to calculate the expected sideslip angle  $\beta_d$  and the expected yaw rate  $\omega_d$ . The linear two-degrees-of-freedom vehicle model shown in

Figure 1 only considered the two degrees of freedom of lateral movement along the y-axis and yaw movement around the z-axis.

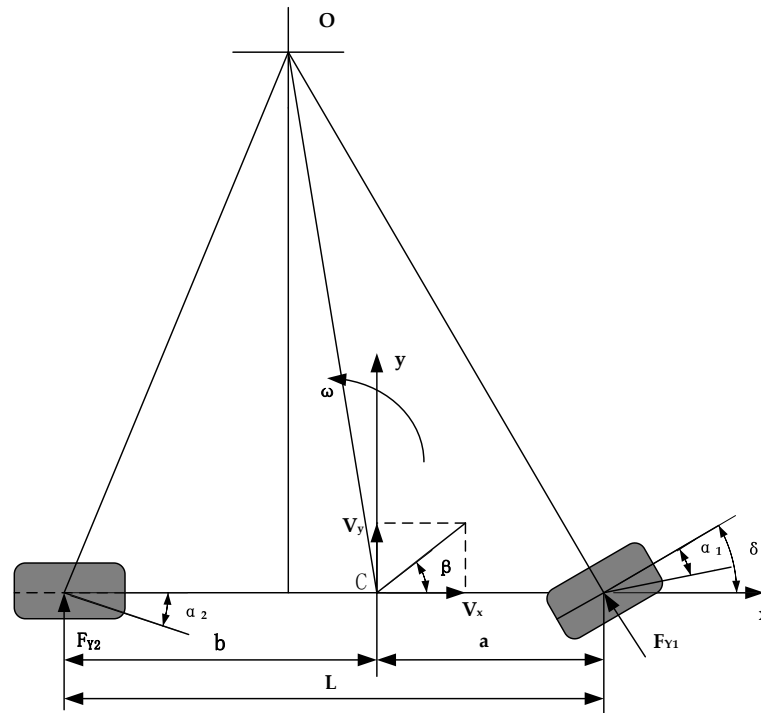


Figure 1. Linear two-degrees-of-freedom vehicle model.

Ignoring the vehicle suspension and keeping the vehicle’s longitudinal speed constant, the cornering characteristics of each tire were in the linear range; therefore, a differential equation of the vehicle motion was derived as follows:

$$\begin{cases} \dot{\omega} = \frac{aC_f - bC_r}{J_Z} \beta + \frac{a^2C_f + b^2C_r}{J_Z v_x} \omega - \frac{aC_f}{J_Z} \delta_f \\ \dot{\beta} = \frac{C_f + C_r}{m v_x} \beta + \left( \frac{aC_f - bC_r}{m v_x^2} - 1 \right) \omega - \frac{C_f}{J_Z} \delta_f \end{cases} \quad (1)$$

where  $a$  and  $b$  are the distance from the center of mass of the vehicle to the front and rear axles,  $L$  is the wheelbase,  $m$  is vehicle mass,  $C_f$  and  $C_r$  are the cornering stiffness of the front and rear axles of the vehicle,  $J_Z$  is the moment of inertia of the vehicle around the z-axis,  $v_x$  is the longitudinal speed of the vehicle,  $\delta_f$  is the front wheel steering angle of the vehicle,  $\beta$  is the sideslip angle of the center of mass, and  $\omega$  is the yaw rate.

The following equalities are true during the vehicle’s steady driving state:

$$\begin{cases} \dot{\omega} = 0 \\ \dot{\beta} = 0 \end{cases} \quad (2)$$

In addition,  $K$  is the stability factor, which is an important parameter that characterizes the steady-state response of the vehicle. The value of  $K$  is obtained using the following formula:

$$K = \frac{m}{L^2} \left( \frac{a}{C_r} - \frac{b}{C_f} \right)$$

After combining Formulas (1) and (2), we obtained

$$\begin{cases} \omega_d = \frac{v_x}{L(1+Kv_x^2)} \delta_f \\ \beta_d = \frac{bLC_r + mav_x^2}{L^2C_r(1+Kv_x^2)} \delta_f \end{cases} \quad (3)$$

In addition, considering the limitation of the road adhesion coefficient on the steady-state maximum of the yaw velocity and the vehicle’s side deflection angle of the linear 2-DOF model, the current road adhesion coefficient was selected as the desired parameter. On a road with a pavement adhesion coefficient of  $\mu$ , the boundary values of the yaw rate  $\omega_{bound}$  and the vehicle’s sideslip angle  $\beta_{bound}$  [14] were calculated as follows:

$$\begin{cases} \omega_{bound} = 0.85 \frac{\mu g}{v_x} \\ |\beta_{bound}| \leq \arctan(0.02 \mu g) \end{cases} \quad (4)$$

where  $g$  is the acceleration due to gravity.

After combining Formulas (4) and (5), we obtained

$$\begin{cases} \omega_d = \min \left\{ \frac{v_x}{L(1+Kv_x^2)} \delta_f, \omega_{bound} \right\} \\ \beta_d = \min \left\{ \frac{bLC_r + mav_x^2}{L^2C_r(1+Kv_x^2)} \delta_f, \beta_{bound} \right\} \end{cases} \quad (5)$$

### 2.2. Vehicle Model

In order to design and verify the distributed drive control strategy, it was necessary to establish a wheel-side rear-drive electric bus model.

This study mainly investigated the lateral driving stability of an electric bus, ignoring the pitch and roll motion of the vehicle, and only considered the five degrees of freedom of the vehicle’s lateral, longitudinal, yaw, and rotational motion of the four wheels. As shown in Figure 2, the simplified five-degrees-of-freedom model was used to analyze the rear-drive forces of the vehicle in direct yaw moment control.

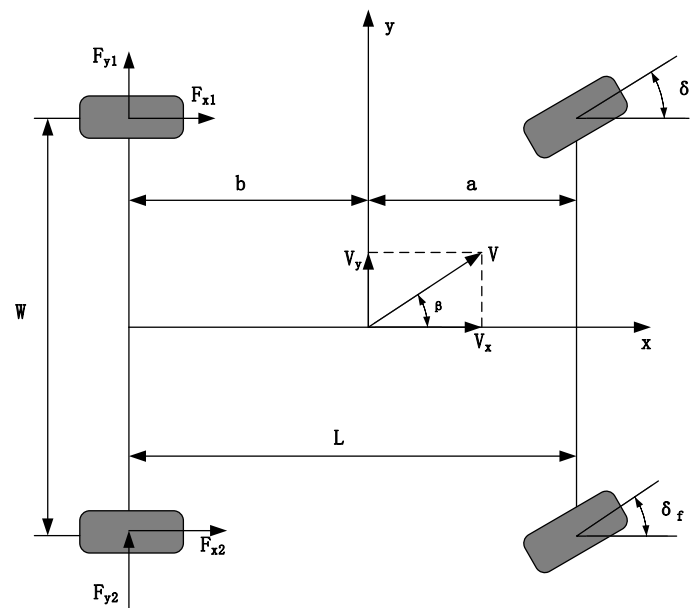


Figure 2. Five-degrees-of-freedom kinematics scheme.

Longitudinal motion equation:

$$m(\dot{V}_x - V_y\omega) = F_{x1} + F_{x2} \quad (6)$$

Lateral motion equation:

$$m(\dot{V}_y + V_x\omega) = F_{y1} + F_{y2} \quad (7)$$

Yaw motion equation:

$$J_Z\omega = \frac{w}{2}(F_{x2} - F_{x1}) - b(F_{y1} + F_{y2}) \quad (8)$$

In the above formulas,  $m$  is the mass of the vehicle;  $V_x$  is the longitudinal velocity of the vehicle;  $V_y$  is the lateral velocity of the vehicle;  $J_Z$  is the moment of inertia of the vehicle around the  $z$ -axis;  $\omega$  is the vehicle's yaw rate;  $a$  is the distance from the center of mass to the front axle;  $b$  is the distance from the center of mass to the rear axle;  $w$  is the rear axle track; and  $F_{x1}$ ,  $F_{x2}$ ,  $F_{y1}$ , and  $F_{y2}$  are, respectively, the longitudinal and lateral reaction forces of the left and right driving wheels on the ground.

From the principle diagram of wheel rotation dynamics shown in Figure 3, the wheel rotation dynamics equation can be obtained as follows:

$$I_w\dot{\omega}_r = T_d - T_b + F_x R \quad (9)$$

where  $I_w$  is the rotational inertia of the wheel,  $R$  is the wheel rolling radius,  $F_x$  is the wheel friction,  $T_d$  is the wheel driving torque, and  $T_b$  is the wheel braking torque.

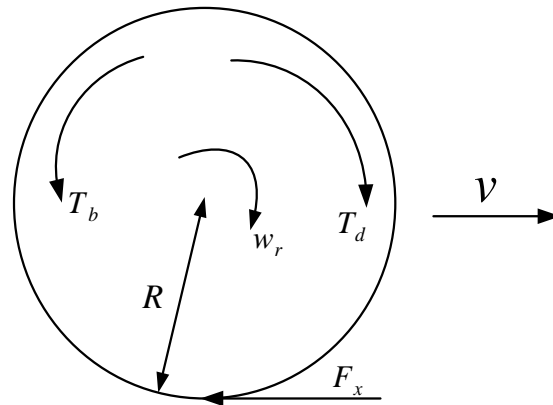


**Figure 3.** Principle diagram of wheel rotation dynamics.

TruckSim vehicle dynamics simulation software was used to build a complete electric bus model. TruckSim can build a nonlinear vehicle model in a parameterized manner as a control strategy simulation verification platform. Some parameters of the electric bus model are shown in Table 1.

**Table 1.** Reference values for some parameters of an electric bus.

Name of the Parameter	Reference Value	Unit	Purpose
Vehicle mass ( $m$ )	12,800	kg	Determine the mass of the vehicle
Length $\times$ width $\times$ height	12,000 $\times$ 2500 $\times$ 3150	mm	Determine the length, width, and height of the vehicle
Height of the center of mass ( $h$ )	1200	mm	
Distance from the center of mass to the front axle ( $a$ )	3240	mm	Determine the center of mass of the vehicle
Distance from the center of mass to the rear axle ( $b$ )	1260	mm	
Wheelbase ( $L$ )	4500	mm	Determine wheelbase
The front tire cornering stiffness $C_f$	119,283.4	N/rad	Determine the vehicle front and rear wheel sideslip stiffness for the calculation of the sideslip force to pave the way
The rear tire cornering stiffness $C_r$	225,781.4	N/rad	
Rear wheel pitch ( $W$ )	1863	mm	To calculate the yaw torque

### 3. Adaptive Distributed Drive Control System Design

For a distributed rear-drive electric bus, designing a reasonable driving force control strategy according to various driving conditions can improve the driving stability and driving safety of the bus. Based on the compensation of the yaw moment, this study designed an adaptive rear driving force distribution control strategy to maintain the body attitude and driving route of an electric bus. The control strategy structure was divided into two layers, namely, an additional yaw moment setting layer and a driving torque distribution layer, as shown in Figure 4.

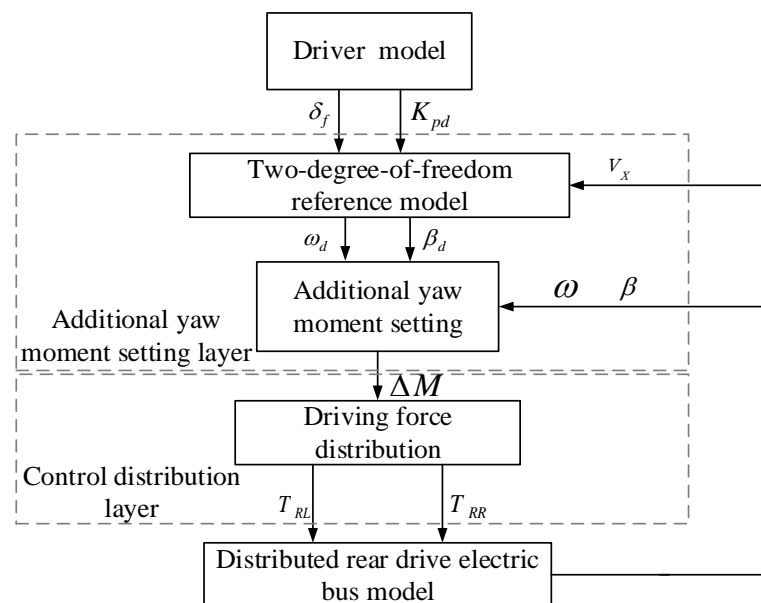


**Figure 4.** Additional yaw moment setting layer and driving torque distribution layer.

The additional yaw moment setting layer inputs the received driver information  $\delta_f$  and  $K_{pd}$  into the reference vehicle model to obtain the expected yaw rate and sideslip angle. The expected yaw rate and sideslip angle are compared with the actual yaw rate and sideslip angle, respectively, and the additional yaw moment is obtained by the adaptive fuzzy controller and input to the next layer. In the driving force distribution layer, the driving forces are reasonably distributed on the left and right rear wheels of the electric bus according to the additional yaw moment constraint.

### 3.1. Additional Yaw Moment Calculation Based on Fuzzy Controller

Fuzzy control is a modern control method that does not rely on the precise mathematical model of the control object. Its structure mainly includes three modules, namely, the fuzzification input, fuzzy reasoning, and anti-fuzzification output, as shown in Figure 5.

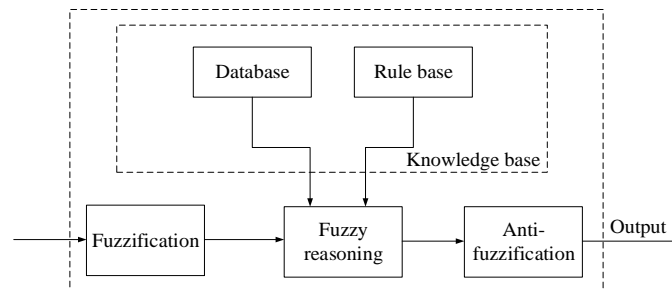


Figure 5. Fuzzy control architecture.

The deviations between the actual values  $\omega$  and  $\beta$  and the expected values  $\omega_d$  and  $\beta_d$  of the yaw rate and the sideslip angle, respectively, are taken as the two input variables of the fuzzy controller. The output of the controller is the additional yaw moment  $\Delta M$  that makes the actual values of the yaw rate and the sideslip angle of the bus follow the expected value. The fuzzy control system block diagram is shown in Figure 6.

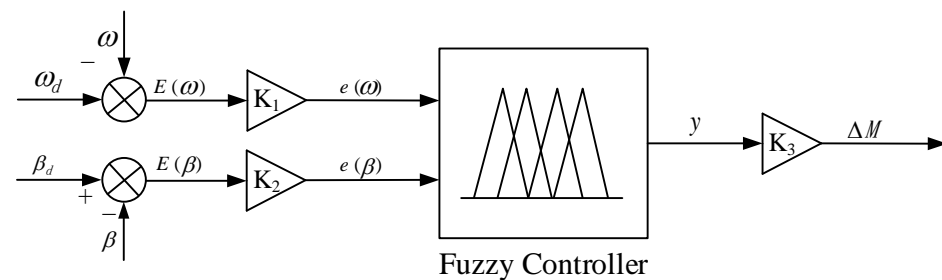


Figure 6. Additional yaw moment calculation based on a fuzzy controller.

In Figure 6, the input  $E = [E(\omega), E(\beta)]^T$  gives the true deviation of the actual value of the yaw rate and the sideslip angle from the expected value, which is the basic domain of fuzzy control.  $e = [k_1 \cdot E(\omega), k_2 \cdot E(\beta)]^T = [e(\omega), e(\beta)]^T$  is the input after the fuzzification process. The fuzzification process is the input variable transformed from the basic domain to the corresponding fuzzy set domain, that is, it multiplies the input variable by the corresponding quantization factor. The relevant sets are as follows:

$$T[e(\omega)] = \{A_{\omega}^1, A_{\omega}^2, \dots, A_{\omega}^n\} \tag{10}$$

$$T[e(\beta)] = \{A_{\beta}^1, A_{\beta}^2, \dots, A_{\beta}^n\} \tag{11}$$

Among them,  $A_{\omega}^j$  and  $A_{\beta}^j$  ( $j = 1, 2, \dots, n$ ) are divided into the  $j$ th fuzzy variable values of  $e(\omega)$  and  $e(\beta)$ , which are defined in the universe of the  $U_{\omega}$  and  $U_{\beta}$  fuzzy collection. The corresponding membership functions are

$$u_{A_{\omega}^j}[e(\omega)](j = 1, 2, \dots, n) \tag{12}$$

$$u_{A_{\beta}^j}[e(\beta)](j = 1, 2, \dots, n) \tag{13}$$

The output is also a fuzzy language variable:

$$T(y) = \{B^1, B^2, \dots B^n\} \tag{14}$$

where  $B^j (j = 1, 2, \dots n)$  is the  $j^{\text{th}}$  fuzzy variable value of  $y$ , which is a fuzzy set defined on the universe  $U_y$ , and the corresponding membership function is  $u_{B^j}(y)$ .

Suppose the corresponding fuzzy rules of the input–output relationship described are  $R_i$  : if  $e(\omega) = A_\omega^1$  and  $e(\beta) = A_\beta^1$  then  $y = B^1$ , and  $i = (1, 2, \dots, n)$ , where  $n$  is the total number of fuzzy rules.

The input quantity adopts the fuzzification method of a single-point fuzzy set. For a given  $e = [e(\omega), e(\beta)]^T$ , the applicability of each rule can be obtained using

$$\alpha_i = u_{A_\omega^i}[e(\omega)]u_{A_\beta^i}[e(\beta)] \tag{15}$$

Through fuzzy reasoning, the membership function of the fuzzy set of the output of each rule can be obtained using

$$u_{B^j}(y) = \alpha_i u_{B^j}(y) \tag{16}$$

Thus, the output total fuzzy set is

$$B = U_{i=1}^n B_i \tag{17}$$

$$u_B(y) = V_{i=1}^n u_{B^i}(y) \tag{18}$$

Taking the weighted average method as the anti-fuzzification method, the output can be obtained using

$$y = \frac{\sum_{i=0}^n y_{c_i} u_{B_i}(y_{c_i})}{\sum_{i=0}^n u_{B_i}(y_{c_i})} \tag{19}$$

where  $y_{c_i}$  is the maximum point taken by  $u_{B_i}(y)$ , which is generally the center point of the membership function. Obviously:

$$u_{B_i}(y_{c_i}) = \max\{u_{B_i}(y)\} = \alpha_i \tag{20}$$

Therefore, the output expression is

$$y = \frac{\sum_{i=0}^n y_{c_i} \alpha_i}{\sum_{i=0}^n \alpha_i} = \frac{\sum_{i=0}^n y_{c_i} u_{A_\omega^i}[k_1 \cdot E(\omega)] u_{A_\beta^i}[k_2 \cdot E(\beta)]}{\sum_{i=0}^n u_{A_\omega^i}[k_1 \cdot E(\omega)] u_{A_\beta^i}[k_2 \cdot E(\beta)]} \tag{21}$$

It can be known from the control algorithm of fuzzy control that

$$\Delta M = y \cdot K_3 \tag{22}$$

$$y = f_1(e(\omega), e(\beta)) = f_1(E(\omega) \cdot K_1, E(\beta) \cdot K_2) \tag{23}$$

In the above Formula (23),  $f_1(\cdot)$  is the functional relationship between the input and output of the fuzzy control system, which is determined by the parameters of the fuzzy controller and the anti-fuzzification method. From Formulas (22) and (23), it can be found that  $\Delta M$  depends not only on the input deviations  $E(\omega)$  and  $E(\beta)$  but also on the size of the quantization factors  $K_1$  and  $K_2$  and the scale factor  $K_3$ . Choosing different quantization factors and scale factors has a great influence on the control effect of the fuzzy control system.

At present, in engineering control, the quantization factors  $K_1$  and  $K_2$  and the scale factor  $K_3$  in the fuzzy control of two-dimensional input and single output is mainly determined using Formulas (24)–(26) [15]:

$$K_1 = \frac{p}{|E_{1max}|} \quad (24)$$

$$K_2 = \frac{n}{|E_{2max}|} \quad (25)$$

$$K_3 = \frac{|\varepsilon_{max}|}{l} \quad (26)$$

In the above formulas,  $E_{1max}$  and  $E_{2max}$  are the maximum deviation of the input quantity, and  $\varepsilon_{max}$  is the precise value of the output control quantity.  $p$  and  $n$  are the numbers of grades in the fuzzy set universe of the two inputs, and  $l$  is the number of grades in the fuzzy set universe of the output. In the formulation process of the additional yaw moment based on fuzzy control, the weighted average method was used as the anti-fuzzification as Formula (21); thus, the magnitude of the additional yaw moment  $\Delta M$  is

$$\Delta M = K_3 \cdot \frac{\sum_{i=0}^n y_{c_i} u_{A_{\omega}^i} [k_1 \cdot E(\omega)] u_{A_{\beta}^i} [k_2 \cdot E(\beta)]}{\sum_{i=0}^n u_{A_{\omega}^i} [k_1 \cdot E(\omega)] u_{A_{\beta}^i} [k_2 \cdot E(\beta)]} \quad (27)$$

In the above fuzzy control, the values of the quantization factors  $K_1$  and  $K_2$  and the scale factor  $K_3$  will not be changed after being determined, and thus, the change range of the controller's output  $\Delta M$  is small. As a result, the adjustment range of the yaw moment of the bus becomes smaller; it cannot adapt to all the driving conditions of the bus.

From the above analysis, it can be learned that the size of the quantization factors and scale factors has a great influence on the control effect of fuzzy controllers. Theoretically, if the quantization factor is increased, it is equivalent to narrowing the basic field of deviation variables and increasing the control effect of the deviation. If the quantization factor is reduced, the control system will not detect the magnitude of the input change when the change in input deviation is not large, which will produce a dead zone of fuzzy control and reduce the control accuracy. When the scale factor increases, the magnification of the system increases and the system responds more quickly. When the scale factor is small, the transition time of the system is long and the steady-state precision becomes poor [16].

### 3.2. Additional Yaw Moment Calculation Based on an Adaptive Fuzzy Controller

Aimed at the problem of vehicle driving lateral stability control caused by the unadjustable quantization factor and scale factor, this study proposed an adaptive fuzzy controller, which dynamically adjusted the quantization factor and scale factor to calculate additional yaw moments according to different vehicle driving conditions.

By analyzing the lateral stability of the vehicle, it can be seen that the degree of control of the yaw rate and the sideslip angle of the center of mass will change with different driving conditions of the vehicle [17].

When an electric bus drives on a high-adhesion road, there is a small deviation between the actual values  $\omega$  and  $\beta$  and the expected values  $\omega_d$  and  $\beta_d$  of the yaw rate and sideslip angle, respectively. By increasing the quantization and scale factors, the actual values  $\omega$  and  $\beta$  of the yaw rate and sideslip angle of the bus follow the expected values  $\omega_d$  and  $\beta_d$  within a short time. When the electric bus drives on a low-adhesion road, there is a larger deviation between the actual values  $\omega$  and  $\beta$  and the expected values  $\omega_d$  and  $\beta_d$  of the yaw rate and sideslip angle. By increasing the quantization factor and reducing the scale factor, the torque difference between the left and right rear wheels is not large, which allows for easier driving on low-adhesion roads. The structure of the adaptive fuzzy controller is shown in Figure 7.

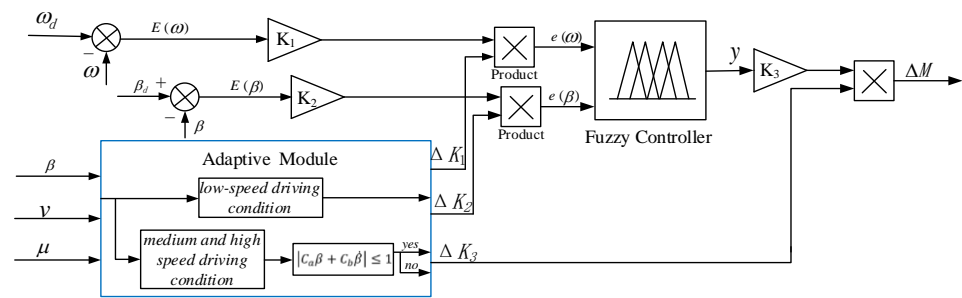


Figure 7. Additional yaw moment calculation based on an adaptive fuzzy controller.

It can be known from the control algorithm of adaptive fuzzy control that

$$\begin{cases} e(\omega) = (K_1 + \Delta K_1) \cdot E(\omega) \\ e(\beta) = (K_2 + \Delta K_2) \cdot E(\beta) \end{cases} \tag{28}$$

$$y = f_2(e(\omega), e(\beta)) \tag{29}$$

The  $f_2(\cdot)$  in the above Formula (29) is the functional relationship between the input and output of the adaptive fuzzy control system, which is determined by the controller parameters and anti-fuzzification. It can be seen from Formulas (28) and (29) that the output of the fuzzy controller not only depends on the input deviations  $E(\omega)$  and  $E(\beta)$  and the quantization factors  $K_1$  and  $K_2$  but also depends on the outputs  $\Delta K_1$  and  $\Delta K_2$  of the adaptive module. Similarly, the magnitude of the additional yaw moment  $\Delta M$  depends not only on the scale factor  $K_3$  but also on the output  $\Delta K_3$  of the adaptive module. The magnitude of the additional yaw moment is

$$\Delta M = (K_3 + \Delta K_3) \cdot y = (K_3 + \Delta K_3) \cdot f_2(e(\omega), e(\beta)) \tag{30}$$

During the driving process of the bus, the adaptive module can output the corresponding  $\Delta K_1$ ,  $\Delta K_2$ , and  $\Delta K_3$  values according to the actual driving conditions to adjust the additional yaw moment  $\Delta M$  of the vehicle so that the bus can maintain the best driving status. Considering the calculation speed of the algorithm, the design of the adaptive module is as follows.

The adaptive module can output additional quantization factors  $\Delta K_1$  and  $\Delta K_2$  and scale factor  $\Delta K_3$  according to the vehicle’s driving conditions and the actual yaw rate and sideslip angle of the vehicle to ensure the control effect and response speed. When the bus is turning at low speed, it is considered that the vehicle can be driven stably by controlling the yaw rate. The adaptive module will shield the deviation value of the sideslip angle. At the same time, to improve the response speed of the fuzzy control, it is necessary to increase the control effect of the yaw rate deviation and the total magnification of the system. Therefore, the outputs of the adaptive module are

$$\Delta K_1 > 1, \Delta K_2 = 0, \Delta K_3 > 1 \{ \text{turning at low speed} \} \tag{31}$$

When the bus is turning at medium and high speeds, the sideslip angle and sideslip rate will be limited to the range of  $|C_a\beta + C_b\dot{\beta}| \leq 1$  [18]. In this range, to ensure that the vehicle driving trajectory is the main control object, the response speed of the control system must be considered. The yaw rate control and sideslip angle control are equally important. At the same time, to ensure driving smoothness, the torque difference between the left and right rear wheels should be reduced. Therefore, the inputs of an adaptive module are

$$\Delta K_1 = \Delta K_2 > 1, \Delta K_3 < 1 \{ |C_a\beta + C_b\dot{\beta}| \leq 1, \text{turning at medium and high speed} \} \tag{32}$$

When this range is exceeded, namely,  $|C_a\beta + C_b\dot{\beta}| > 1$ , the only control object is to ensure the vehicle's driving trajectory, and the adaptive module will shield the deviation value of the yaw rate. Therefore, only the sideslip angle control is used to maintain a stable drive, and the outputs of the adaptive module are

$$\Delta K_1 = 0, \Delta K_2 > 1, \Delta K_3 < 1 \left\{ |C_a\beta + C_b\dot{\beta}| > 1, \text{turning at medium and high speed} \right\} \quad (33)$$

According to the analysis of vehicle dynamics stability and reference [19],  $C_a = 4.386$  and  $C_b = 2.562$ .

In this study, the adaptive fuzzy controller fuzzified the precise values of the input deviations  $E(\omega)$  and  $E(\beta)$  into seven fuzzy sets, which were negative big (NB), negative medium (NM), negative small (NS), zero (ZO), positive small (PS), positive medium (PM), and positive big (PB). The output variable  $\Delta M$  was divided into nine fuzzy sets, which were negative very big (NVB), negative big (NB), negative medium (NM), negative small (NS), zero (ZO), positive small (PS), positive medium (PM), positive big (PB), and positive very big (PVB). The following Figures 8–10 show the corresponding membership functions.

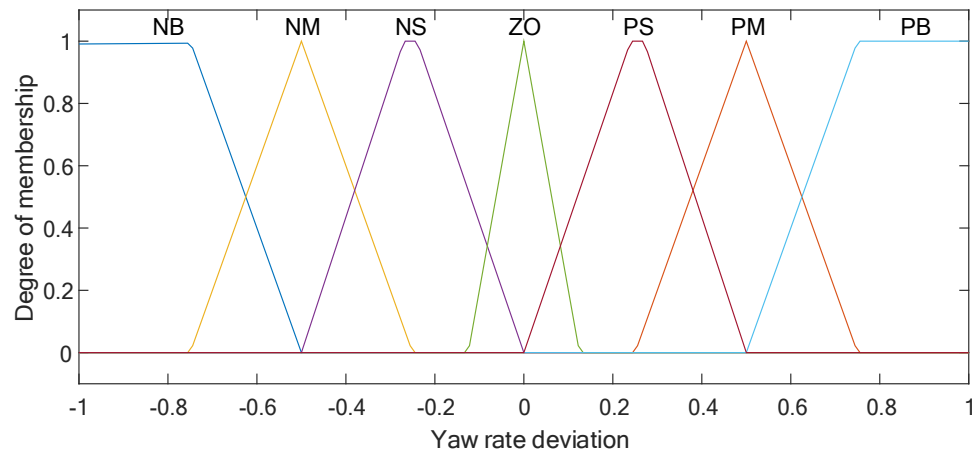


Figure 8. Membership function of the yaw rate deviation.

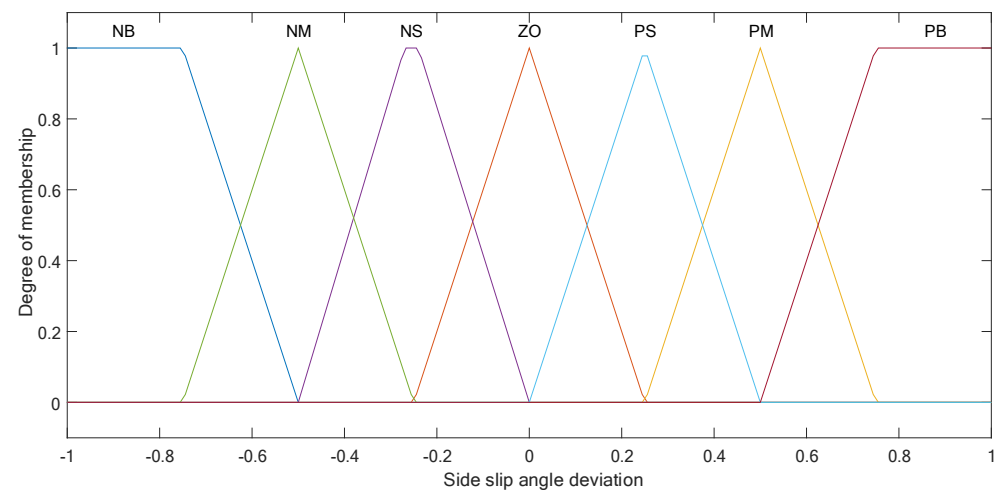


Figure 9. Membership function of the sideslip angle deviation.

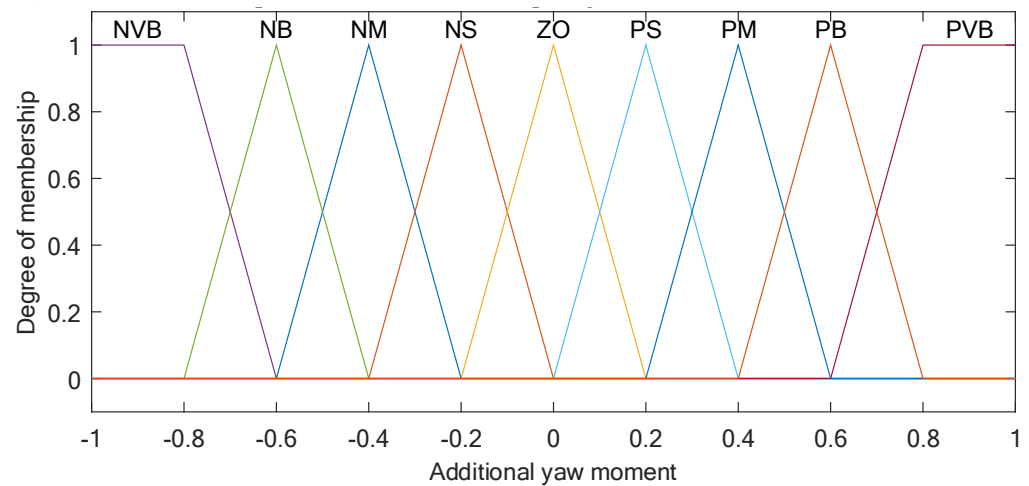


Figure 10. Membership function of the additional yaw moment.

Fuzzy reasoning is the core link in fuzzy control, which is to form a one-to-one rule relationship between the input variable combination of the fuzzy controller and the output variable based on expert experience. The reasoning relationships used in this study are shown in Table 2, with a total of 49 fuzzy rules.

Table 2. Fuzzy control fuzzy rule table.

$e_\omega \setminus e_\beta$	NB	NM	NS	ZO	PS	PM	PB
NB	NVB	NVB	NVB	NB	NB	NM	NB
NM	NB	NB	NB	NM	NM	NS	NS
NS	NB	NM	NM	NM	NS	ZO	ZO
ZO	NM	NM	NS	ZO	ZO	PS	PS
PS	NM	NS	ZO	PS	PS	PM	PM
PM	NS	ZO	PS	PM	PM	PB	PB
PB	ZO	PS	PM	PB	PB	PVB	PVB

In order to obtain the precise value of the output, the output of the fuzzy controller must be anti-fuzzification. Common anti-fuzzification methods include the maximum membership degree method, the area center of gravity method, and the weighted average method. In this study, considering the real-time performance and operation speed of the control algorithm, the weighted average method was selected as the method of anti-fuzzification. The calculation formula of the final additional yaw moment  $\Delta M$  is shown in Formula (34).

$$\Delta M = (K_3 + \Delta K_3) \cdot \frac{\sum_{i=0}^n y_{c_i} u_{A_\omega^i} [(K_1 + \Delta K_1) \cdot E(\omega)] u_{A_\beta^i} [(K_2 + \Delta K_2) \cdot E(\beta)]}{\sum_{i=0}^n u_{A_\omega^i} [(K_1 + \Delta K_1) \cdot E(\omega)] u_{A_\beta^i} [(K_2 + \Delta K_2) \cdot E(\beta)]} \tag{34}$$

### 3.3. Driving Torque Distribution

After the total driving torque  $T_d$  is determined by the accelerator pedal, the driving torque needs to be reasonably distributed to the left and right rear driving wheels. When the vehicle is driving straight, the total driving torque  $T_d$  is equally distributed to the left and right driving wheels. When the vehicle turns, the torques of the left and right drive wheels are no longer equal and satisfy the constraint of additional yaw moment  $\Delta M$  calculated by the adaptive fuzzy control.

By analyzing the driving state of the vehicle, it can be seen that when the vehicle is understeering on the left or oversteering on the right, the right wheel torque should be increased while the left wheel torque should be reduced to ensure the steering stability

of the vehicle; when the vehicle is oversteering on the left or understeering on the right, the left wheel torque should be increased while the right wheel torque should be reduced to ensure the steering stability of the vehicle. Therefore, the torques of the left and right driving wheels should meet the constraints of the following Equation (35):

$$\begin{cases} T_{RR} + T_{RL} = T_d \\ (T_{RR} - T_{RL}) \frac{W}{2R} = \Delta M \end{cases} \quad (35)$$

In the above formula,  $W$  is the rear wheel thread and  $R$  is the rolling radius of the driving wheel.

#### 4. Hardware-in-the-Loop Test

It is usually necessary to perform functional logic testing on the automotive electronic control unit after it has been developed. Hardware-in-the-loop testing is considered to be one of the most important testing methods before real vehicle testing. The hardware-in-the-loop test interacts with a virtual vehicle through real controller hardware and can receive and send the state parameter signals during the driving process of the vehicle in real time. By analyzing the test results, it can effectively monitor the designed control strategy, the operation of the controller, and the control effect of the control strategy. Because of this, hardware-in-the-loop testing has higher confidence than software offline simulation.

The hardware testbed developed by National Instruments (National Instruments company) is compatible with both TruckSim (TruckSim 2020) and Matlab (MATLAB R2020b v9.9.0), making it ideal for building the hardware-in-the-loop testing environment shown in Figure 11. Combined with the hardware foundation of the laboratory, the equipment used for the hardware-in-the-loop test in this study included an industrial control cabinet equipped with an NI PXIE-8880 real-time processor (NI PXIE-8880 real-time processor, National Instruments, Austin, Texas, USA), an NI PXIE-8512 CAN communication board card (NI PXIE-8880 real-time processor, National Instruments, Austin, Texas, USA), and a DSP28335 controller (DSP28335 controller, Texas Instruments, Dallas, Texas, USA). The upper computer control software includes Matlab/Simulink (MATLAB R2020b v9.9.0) and NI Veristand (NI VeriStand 2020 R4 V20.4.0.49152).

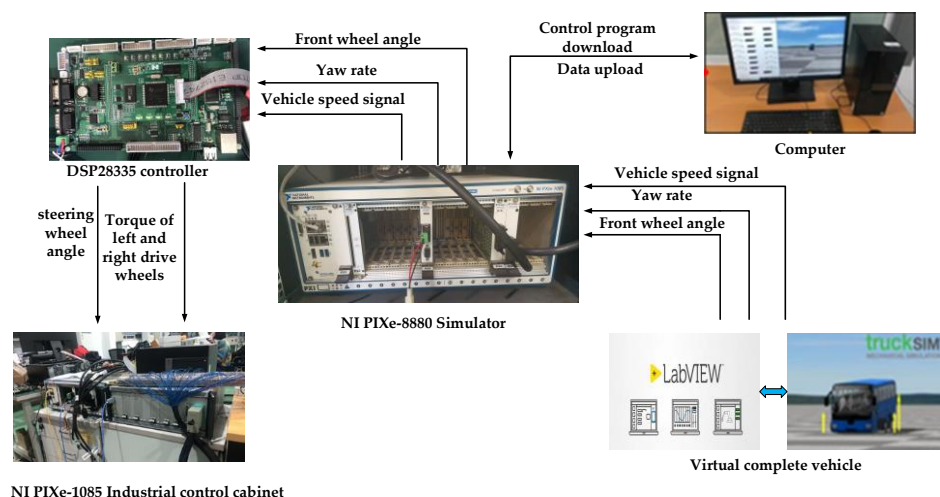


**Figure 11.** Hardware-in-the-loop test platform.

##### 4.1. Large Turning in a Low-Speed Driving Condition

The driving conditions of a vehicle accelerating with a larger steering angle at a lower speed on a good road were simulated. Assuming that the vehicle was driving on a road with an adhesion coefficient of  $\mu = 0.7$ , an initial speed of 30 km/h, and the steering wheel rotated 180° counterclockwise from 6 s, the resulting steering signal is shown in Figure 12. The accelerator pedal was depressed to accelerate at 10 s. The accelerator pedal signal is

shown in Figure 13. In this study, the design of the adaptive fuzzy control did not consider the influence of sideslip angle on driving stability at low speed, and thus, there was no comparison curve of the sideslip angle at low speed. The curves of the vehicle’s speed, yaw rate, and lateral acceleration are shown in Figure 14, and the vehicle’s driving parameters under this driving condition are shown in Table 3.

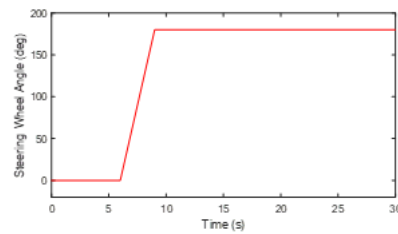


Figure 12. Large steering wheel angle.

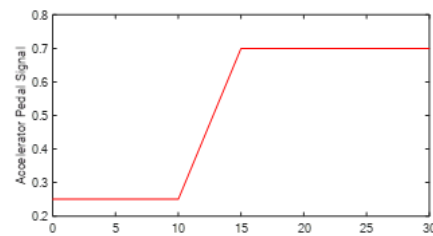


Figure 13. Acceleration pedal.

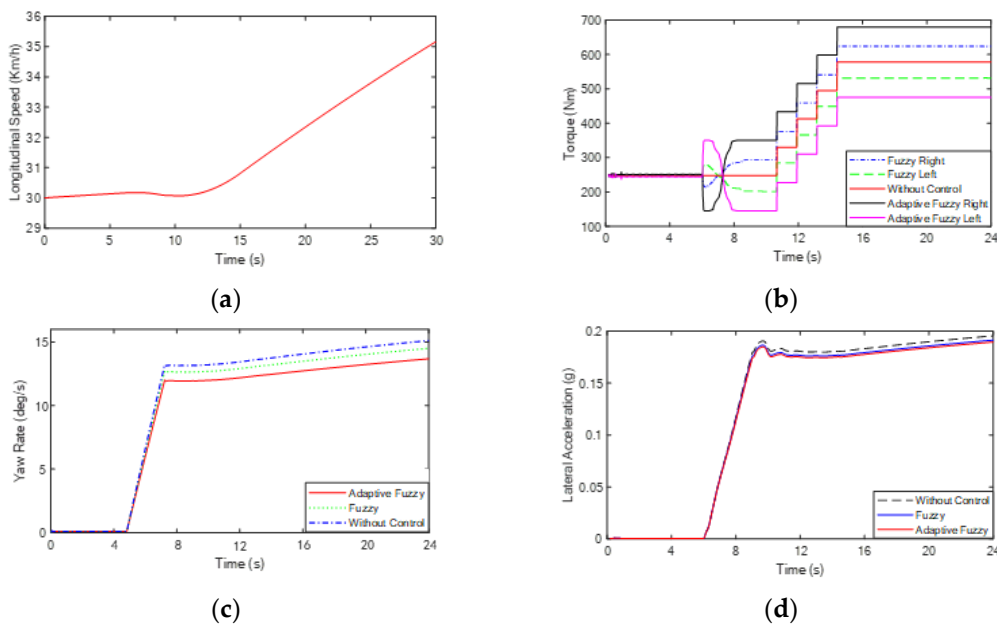


Figure 14. (a) Speed, (b) torque; (c) yaw rate, and (d) lateral acceleration.

Table 3. Comparison of the simulation results with a large steering angle at low speed.

Simulation Conditions	Without Control	Fuzzy Control	Adaptive Fuzzy Control
Maximum yaw rate (deg/s)	15.21	14.51	14.25
Yaw rate deviation rate	18%	12%	10%

As shown in Figure 12, the bus underwent a large steering wheel step test. The bus entered the steering process and the vehicle speed remained unchanged from 6 s to 9 s. After 9 s, the steering wheel angle reached 180 degrees and then it no longer changed. The accelerator pedal opening was increased from 0.25 to 0.7 to cause the vehicle speed to increase and the yaw rate also began to increase. When driving under no control and ordinary fuzzy control, the value of the vehicle yaw rate was significantly larger than that under adaptive fuzzy control and the vehicle had an obvious tendency to oversteer. Under this adaptive fuzzy control strategy, a smaller yaw rate could effectively restrain the vehicle from oversteering and the steering stability of the electric bus was improved. Since the low-speed driving condition was selected, the lateral acceleration of the vehicle did not change much under no control, fuzzy control, and adaptive fuzzy control, as shown in Figure 14d.

Through the analysis of the yaw rate curve, it was not difficult to conclude that compared with no control and fuzzy control, the adaptive fuzzy control could be used under the condition of low speed and large steering of the distributed rear-drive electric bus, where the maximum yaw rate of adaptive fuzzy control is 1.8% lower than that of fuzzy control and 6.3% lower than that of no control. This showed that the adaptive fuzzy control improved the stability of the body of the distributed rear-drive electric bus under the condition of low speed and large steering.

It can be seen that both adaptive fuzzy control and traditional fuzzy control could effectively reduce the maximum response amplitude of the yaw rate error curve. However, adaptive control could further optimize the control effect and better ensure the stability of the vehicle under the condition of low speed and large steering. As can be seen from Table 3, compared with the other two control methods, the vehicle yaw rate deviation under adaptive control was the smallest.

#### 4.2. Small Turning in a High-Speed Driving Condition

The driving condition of a vehicle accelerating with a smaller steering angle at a higher speed on a good road was simulated. Assuming that the vehicle was driving on a road with an adhesion coefficient of  $\mu = 0.85$ , an initial test speed of 80 km/h, and the steering wheel rotated  $50^\circ$  counterclockwise from 6 s, the resulting steering signal is shown in Figure 15. The accelerator pedal was depressed to accelerate at 10 s. The accelerator pedal signal is shown in Figure 16. The vehicle's speed, torque, yaw rate, sideslip angle, and lateral acceleration are shown in Figure 17, and the vehicle's driving parameters under this driving condition are shown in Table 4.

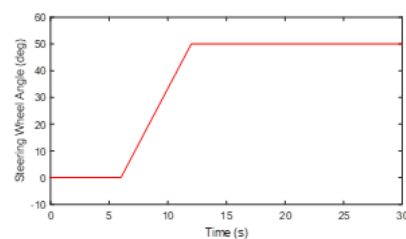


Figure 15. Small steering wheel angle.

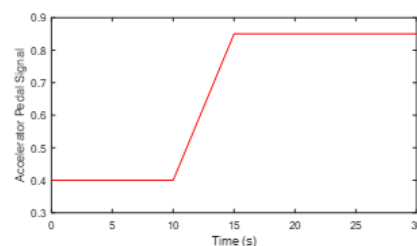


Figure 16. Acceleration pedal.

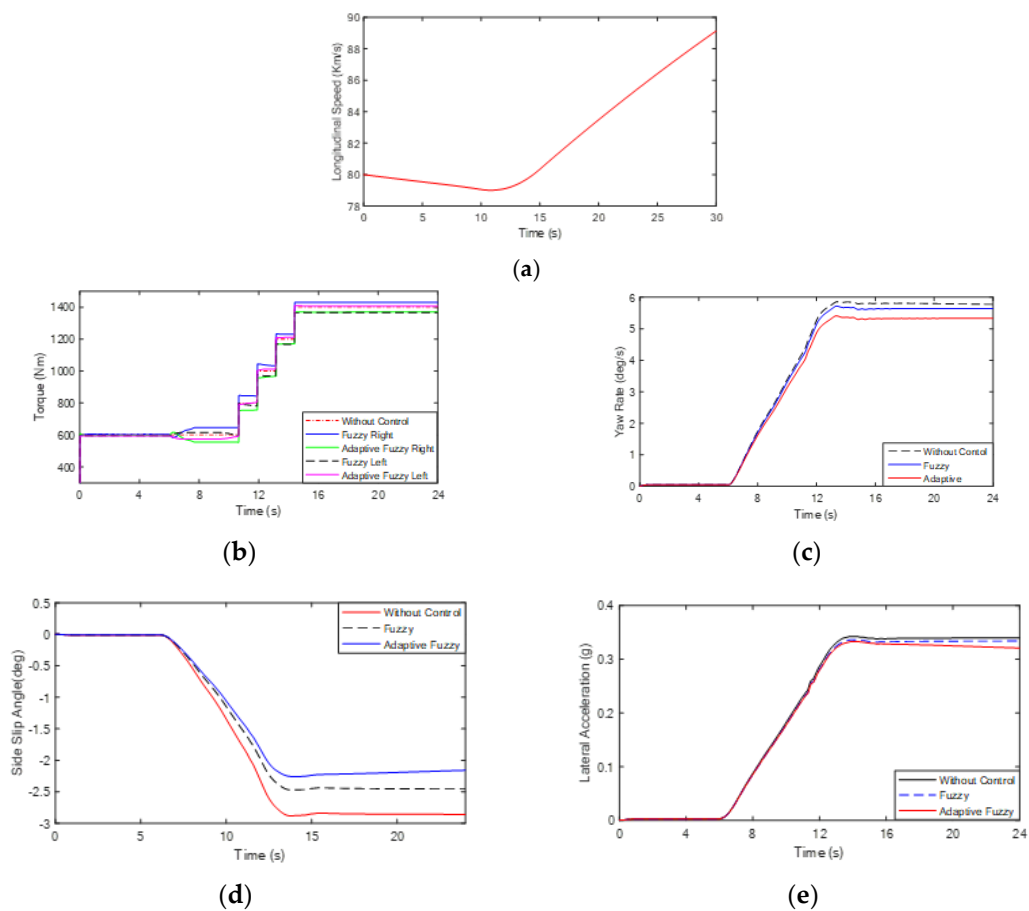


Figure 17. (a) Speed, (b) torque, (c) yaw rate, (d) sideslip angle, and (e) lateral acceleration.

Table 4. Comparison of the simulation results with a small steering angle at high speed.

Simulation Conditions	Without Control	Fuzzy Control	Adaptive Fuzzy Control
Maximum yaw rate (deg/s)	5.53	4.88	4.45
Maximum sideslip angle (deg)	2.8	2.23	2.07
Yaw rate deviation rate	42%	35%	23%
Sideslip angle deviation rate	58%	25%	16%

As shown in Figures 15 and 16, the bus underwent a small steering wheel step test. The bus entered the steering process, and the vehicle’s speed remained unchanged from 6 s to 11 s. After 11 s, the steering wheel angle reached 50 degrees, and then it no longer changed. The accelerator pedal opening was increased from 0.4 to 0.85 to cause the vehicle speed to increase, and the deviation between the actual value of the yaw rate and the expected value began to increase. It can be seen from Figure 17 that when the bus was driving under no control, the actual values of the yaw rate and sideslip angle were much larger than when under control. If the lateral acceleration is too large, the tire lateral force margin is reduced, and the vehicle has a serious tendency to oversteer. Moreover, if the vehicle speed and sideslip angle are relatively large, the vehicle tends to sideslip and drift, and the vehicle is in a very dangerous driving state. Under the fuzzy control strategy, the vehicle’s actual yaw rate, sideslip angle, and lateral acceleration all become smaller, but between 12 s and 30 s, the vehicle’s sideslip angle changed greatly, resulting in large body attitude changes and violent lateral movement, worsening the vehicle ride comfort. Under

the adaptive fuzzy control strategy, the actual values of the yaw rate and sideslip angle were at a minimum, respectively, and the fluctuations were small. It was found that the tendency of the vehicle to oversteer was suppressed and the body attitude remained stable.

Based on the analysis of the yaw rate curve, it was not difficult to conclude that compared with no control and fuzzy control, the adaptive fuzzy control could be used under the condition of high speed and small steering of the distributed rear-drive electric bus, the maximum yaw rate of adaptive fuzzy control was 8.8% lower than that of fuzzy control and 19.5% lower than that of no control. Compared with the traditional fuzzy control, the maximum sideslip angle of the adaptive fuzzy control was reduced by 7.4% and 26%, respectively. This shows that the adaptive fuzzy control improved the stability of the body of the distributed rear-drive electric bus under the condition of high speed and small steering.

It can be seen that both adaptive fuzzy control and traditional fuzzy control could effectively reduce the maximum response amplitude of the yaw rate error curve. However, adaptive control could further optimize the control effect and better ensure the stability of the vehicle under high-speed small steering conditions. As can be seen from Table 4, compared with the other two control methods, the deviation rate between the yaw rate and sideslip angle under adaptive control was the smallest.

#### 4.3. Slalom Test in a Medium-Speed Driving Condition

The driving condition of a vehicle with a slalom test at medium speed on a low-adhesion-coefficient road was simulated. Assuming that the vehicle was driving on a road with an adhesion coefficient of  $\mu = 0.7$ , an initial speed of 60 km/h, and the steering wheel performed a  $120^\circ$  reciprocating steering operation after 6 s, the resulting steering signal is shown in Figure 18. The accelerator pedal opening remained unchanged. The accelerator pedal signal is shown in Figure 19. The curves of the vehicle's speed, torque, yaw rate, and sideslip angle are shown in Figure 20, and the vehicle's driving parameters under these driving conditions are shown in Table 5.

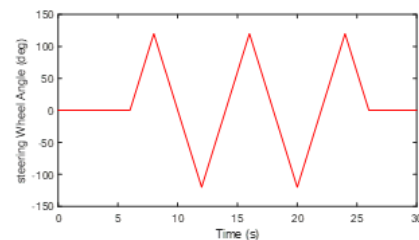


**Figure 18.** Steering wheel angle during the slalom test.

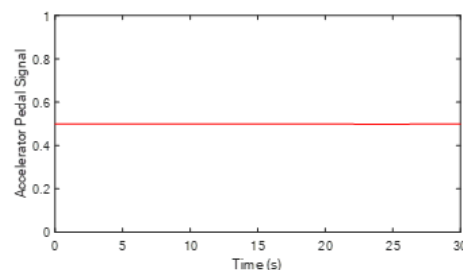


**Figure 19.** Acceleration pedal.

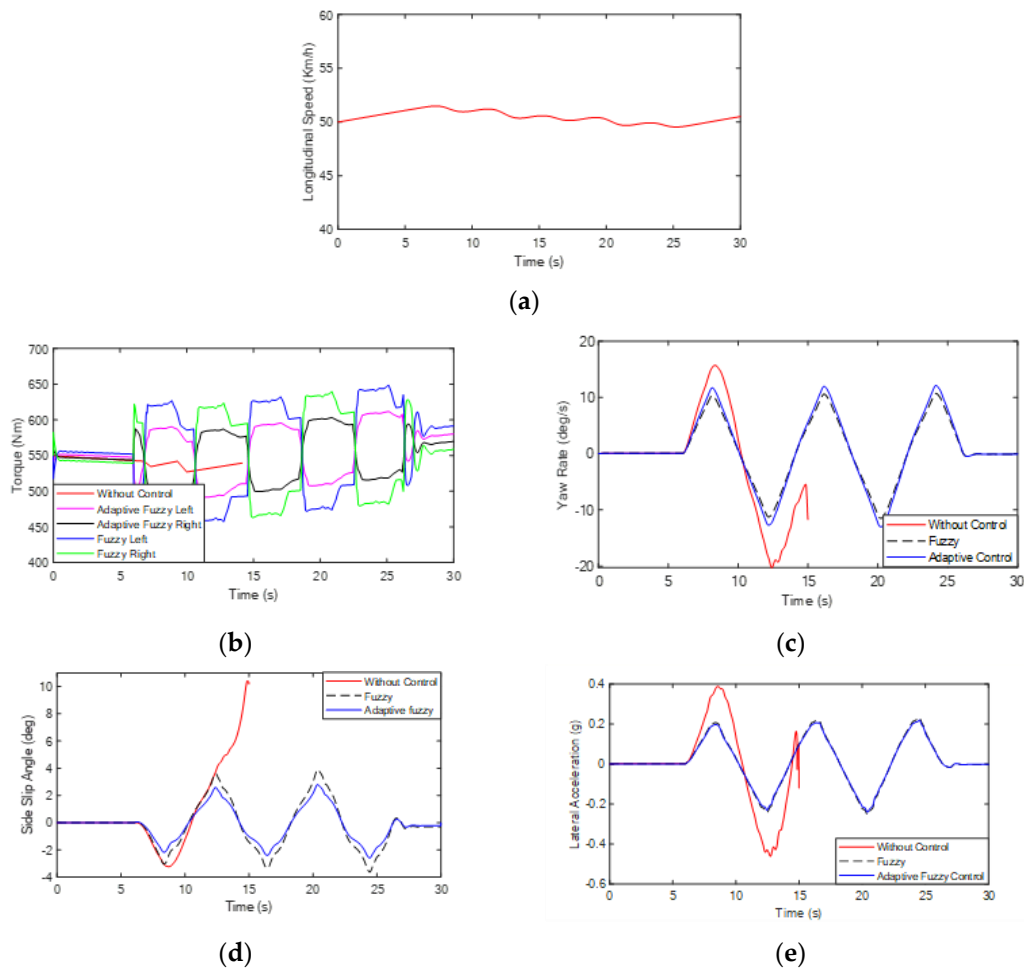


Figure 20. (a) Speed, (b) torque, (c) yaw rate, (d) sideslip angle, and (e) lateral acceleration.

Table 5. Comparison of simulation results from the slalom test at medium speed.

Simulation Conditions	Without Control	Fuzzy Control	Adaptive Fuzzy Control
Maximum yaw rate (deg/s)	−20.1	13.51	11.51
Maximum sideslip angle (deg)	10	4.1	2.6
Yaw rate deviation rate	83%	31%	12%
Sideslip angle deviation rate	852%	38%	15%

As shown in Figures 18 and 19, the bus underwent a slalom test from 6 s to 26 s. The steering wheel signal was a sine wave with a 120° amplitude. The accelerator pedal opening was increased from 0.3 to 0.8 after 10 s to cause an increase in the vehicular speed. As shown in Figure 20, the yaw rate and sideslip angle of the bus sharply increased at 8 s without control, indicating that the bus had become unstable and rolled over. With fuzzy control and adaptive fuzzy control, the actual values of the yaw rate and sideslip angle were reduced, but the tracking effect of the adaptive fuzzy control was more ideal. The yaw rate was larger at the peak of the steering wheel angle, and the sideslip angle fluctuated sharply at 21 s with fuzzy control. With adaptive fuzzy control, deviations of the yaw rate and sideslip angle were only 23% and 16%, respectively, and the driving state of the vehicle was also the most stable.

The simulation results showed that the designed distributed drive control strategy could effectively reduce the sideslip angle and lateral acceleration of the vehicle under

three typical driving conditions, quickly stabilize the yaw rate, and improve the steering stability of the vehicle.

Through the analysis of the yaw rate curve, it was not difficult to conclude that compared with no control and fuzzy control in the distributed rear-drive electric bus under the condition of medium speed, the maximum yaw rate of adaptive fuzzy control was 14.8% lower than that of fuzzy control and 42.7% lower than that of no control. The results showed that the adaptive fuzzy control improved the stability of the body of the distributed rear-drive electric bus under the condition of moderate speed.

It can be seen that both adaptive fuzzy control and traditional fuzzy control could effectively reduce the maximum response amplitude of the yaw rate error curve. However, adaptive control could further optimize the control effect and better ensure the stability of the vehicle at medium speed. As can be seen from Table 5, compared with the other two control methods, the deviation rate of the vehicle sideslip angle under adaptive control was the smallest.

## 5. Conclusions

In this study, an adaptive distributed drive control strategy was proposed. Based on the direct yaw moment control principle and the advantages of independent controllable driving torque of the distributed rear-drive electric bus, the adaptive fuzzy controller was designed to calculate the additional yaw moment, and the optimal driving torques of the left and right rear wheels were obtained through the driving torque distribution rules. Three typical driving conditions of large turning at low speed, small turning at high speed, and slalom testing at medium speed were carried out and analyzed using an HIL test. The simulation results showed that the adaptive distributed drive control reduced the yaw rate deviations in low- and high-speed conditions from 18% and 42% without control to 10% and 23% with control, respectively. Under slalom testing in medium speed conditions, deviations of the yaw rate and sideslip angle with adaptive drive control were reduced from 83% and 852% without control to 12% and 15%, respectively.

Compared with ordinary fuzzy control, the adaptive drive control effectively reduced the lateral acceleration of the vehicle and significantly improved the ability to follow the expected values of the yaw rate and sideslip angle. The lateral stability and ride comfort of the electric bus were greatly enhanced. In the future, real vehicle road tests will be performed to further verify the designed control strategy.

**Author Contributions:** Conceptualization and methodology, H.C.; investigation and formal analysis, J.G.; validation and writing—original draft preparation, S.C. and W.W. (Weiyang Wang); supervision and writing—review and editing, W.W. (Wei Wei); funding acquisition, S.Z. and R.Z. All authors have read and agreed to the published version of the manuscript.

**Funding:** We gratefully acknowledge the financial support of this research by the following projects: Research on the theory and method of the autonomous cooperative operation control of high-speed trains (Grant No. U1934221) and Research and manufacture of a high-precision grinding process of wear-resistant seals of construction machinery (Grant No. ZDLQ2021005).

**Data Availability Statement:** Not applicable.

**Conflicts of Interest:** The authors declare no conflict of interest.

## References

1. Koibuchi, K.; Yamamoto, M.; Fukada, Y.; Inagaki, S. Vehicle stability control in limit cornering by active brake. *JSAE Review* **1996**, *16*, 323.
2. Fujimoto, H.; Takahashi, N.; Tsumasaka, A.; Noguchi, T. Motion control of electric vehicle based on cornering stiffness estimation with yaw-moment observer. In Proceedings of the 9th IEEE International Workshop on Advanced Motion Control, Istanbul, Turkey, 27–29 March 2006.
3. Li, Y.; Zhang, J.; Guo, K.; Wu, D. A Study on Force Distribution Control for the Electric Vehicle with Four in-Wheel Motors; SAE Technical Paper. Available online: <https://www.sae.org/publications/technical-papers/content/2014-01-2379/> (accessed on 20 October 2022).

4. Mokhiamar, O.; Abe, M. How the four wheels should share forces in an optimum cooperative chassis control. *Control. Eng. Pract.* **2006**, *14*, 295–304. [[CrossRef](#)]
5. Yu, Z.P.; Feng, Y.; Xiong, L. Review on vehicle dynamics control of distributed drive Electric vehicle. *Jixie Gongcheng Xuebao (Chin. J. Mech.Eng.)* **2013**, *49*, 105–114. [[CrossRef](#)]
6. Xia, C.L. *Research on Control Method of Chassis Dynamics Based on the Longitudinal Forces Distribution and Active Steering*; Tongji University: Shanghai, China, 2007.
7. Jonasson, M.; Andreasson, J.; Solyom, S.; Jacobson, B. Utilization of actuators to improve vehicle stability at the limit: From hydraulic brakes towards electric propulsion. *J. Dyn. Syst. Meas. Control. Trans. ASME* **2011**, *133*, 51003.1–51003.10. [[CrossRef](#)]
8. Fujimoto, H.; Saito, T.; Noguchi, T. Motion stabilization control of electric vehicle under snowy conditions based on yaw-moment observer. In Proceedings of the 8th IEEE International Workshop on Advanced Motion Control, Kawasaki, Japan, 28 March 2004; pp. 35–40.
9. Qiu, H.; Zhang, H.; Min, L.; Ma, T.; Zhang, Z. Adaptive Control Method of Sensorless Permanent Magnet Synchronous Motor Based on Super-Twisting Sliding Mode Algorithm. *Electronics* **2022**, *11*, 3046. [[CrossRef](#)]
10. Grabski, P.; Jaśkiewicz, M.; Jurecki, R.; Kurczyński, D.; Łagowski, P.; Stańczyk, T.L.; Szumska, E.; Zuska, A. Lateral acceleration tests during circular driving maneuvers and double lane change. *IOP Conf. Ser. Mater. Sci. Eng.* **2022**, *1247*, 012009. [[CrossRef](#)]
11. Chang, H.; Cheng, L. Simulation Calculation of Air Conditioning System Under Complex Vehicle Conditions. *E3S Web Conf.* **2021**, *233*, 04024. [[CrossRef](#)]
12. Shao, K.; Zheng, J.; Yang, C.; Xu, F.; Wang, X.; Li, X. Chattering-free adaptive sliding-mode control of nonlinear systems with unknown disturbances. *Comput. Electr. Eng.* **2021**, *96*, 107538. [[CrossRef](#)]
13. Giap, N.D.; Thien, T.D.; Kwan, A.K. Disturbance Observer-Based Chattering-Attenuated Terminal Sliding Mode Control for Nonlinear Systems Subject to Matched and Mismatched Disturbances. *Appl. Sci.* **2021**, *11*, 8158. [[CrossRef](#)]
14. Rajamani, R. *Vehicle Dynamics and Control*; Springer: New York, NY, USA, 2016; pp. 61–69.
15. King, P.J.; Mamdani, E.H. The application of fuzzy control systems to industrial processes. *Automatica* **1977**, *13*, 235–242. [[CrossRef](#)]
16. Yun, J.; Sun, Y.; Li, C.; Jiang, D.; Tao, B.; Li, G.; Liu, Y.; Chen, B.; Tong, X.; Xu, M. Self-adjusting force/bit blending control based on quantitative factor-scale factor fuzzy-PID bit control. *Alex. Eng. J.* **2022**, *61*, 4389–4397. [[CrossRef](#)]
17. Kati, M.S.; Fredriksson, J.; Jacobson, B.; Laine, L. A feedback-feed-forward steering control strategy for improving lateral dynamics stability of an A double vehicle at high speeds. *Veh. Syst. Dyn.* **2022**, *60*, 3955–3976. [[CrossRef](#)]
18. Elvis, V.; Basilio, L.; Aleksandr, S. Cross-combined UKF for vehicle sideslip angle estimation with a modified Dugoff tire model: Design and experimental results. *Meccanica* **2021**, *56*, 2653–2668.
19. Ryu, J.; Lee, J.-S.; Kim, H. Evaluation of A Direct Yaw Moment Control Algorithm by Brake Hardware-in-the-Loop Simulation. *Korean Soc. Automot. Eng.* **1999**, *7*, 172–179.